Photocorrosion-Limited Maximum Efficiency of Solar Photoelectrochemical Water Splitting

Ling-Ju Guo,[1] Jun-Wei Luo,[2,3,*] Tao He,[1] Su-Huai Wei,[4] and Shu-Shen Li[2,3]

[1] *Chinese Academy of Sciences (CAS) Key Laboratory of Nanosystem and Hierarchy Fabrication, CAS Center for Excellence in Nanoscience, National Center for Nanoscience and Technology, Beijing 100190, China*

[2] *State key laboratory of superlattices and microstructures, Institute of Semiconductors, Chinese Academy of Sciences, Beijing 100083, China*

[3] *Center of Materials Science and Optoelectronics Engineering, University of Chinese Academy of Sciences, Beijing 100049, China*

[4] *Beijing Computational Science Research Center, Beijing 100094, China*

(Received 3 June 2018; revised manuscript received 4 September 2018; published 27 December 2018)

Photoelectrochemical (PEC) water splitting to generate hydrogen is one of the most studied methods for converting solar energy into clean fuel because of its simplicity and potentially low cost. Despite over 40 years of intensive research, PEC water splitting remains in its early stages with stable efficiencies far less than 10%, a benchmark for commercial applications. We reveal that the desired photocorrosion stability sets a limit of 2.48 V [relative to the normal hydrogen electrode (NHE)] for the highest possible potential of the valence band (VB) edge of a photocorrosion-resistant semiconducting photocatalyst. This limitation excludes semiconducting photocatalysts with band gap less than 2.48 eV for PEC water splitting. We further demonstrate that such a limitation has deep roots in the underlying physics after deducing the relation between the energy position of the VB edge and free energy for a semiconductor. The disparity between the stability-limited VB potential at 2.48 V and the oxygen evolution reaction (OER) potential at 1.23 V vs NHE reduces the maximum solar-to-hydrogen (STH) conversion efficiency from common thought 30.7% to approximately 8% for long-term stable single-band-gap PEC water-splitting cells. Based on this understanding, we suggest that the most promising strategy to overcome this 8% efficiency limit is to decouple the requirements of efficient light harvesting and chemical stability by protecting the active semiconductor photocatalyst surface with a photocorrosion-resistant oxide coating layer.

DOI: 10.1103/PhysRevApplied.10.064059

I. INTRODUCTION

Photoelectrochemical (PEC) cells that do not use an external bias or sacrificial reagents are of interest because of their simplicity and potentially low fabrication costs [1–4]. A PEC cell is based on a semiconductor-liquid junction, where free carriers (electrons and holes) generated by light absorption in the semiconductor are driven into the solution by the electric field at the junctions. Specifically, for a *n* type semiconductor photocatalyst PEC cell, photogenerated holes initiate the oxygen evolution reaction (OER) at the surface of the semiconductor electrode and oxidize water to oxygen; photogenerated electrons entering the counter electrode drive the hydrogen evolution reaction (HER) and reduce water to hydrogen. A semiconducting material that can efficiently absorb sunlight to generate electron-hole pairs and that has a high mobility and long lifetime to prevent electron-hole recombination within the material before the electron-hole pairs reach the junction is needed to achieve efficient solar-to-hydrogen (STH) conversion. Additionally, the band gap of a semiconductor photocatalyst must straddle the HER and OER potentials [1] to create favorable reaction kinetics toward overall water splitting. In other words, the potential of the conduction band (CB) edge (ϕ^{CB}) must be more negative than the HER potential ($\phi^0(H^+/H_2) = 0$ V vs the normal hydrogen electrode (NHE), which is approximately 4.5 eV below the vacuum level; and the potential of the valence band (VB) edge (ϕ^{VB}) must be more positive than the OER potential [$\phi^0(H_2O/O_2) = 1.23$ V vs NHE]. In addition to exhibiting an optimal band gap for harnessing sufficient sunlight and favorable band-edge positions for driving overall water splitting, a semiconductor photocatalyst must also exhibit excellent stability in aqueous solution, which is the main limiting factor for the use of conventional photovoltaic semiconductors as photocatalysts [1–5] and thus, is the main challenge to realizing high STH efficiency for water splitting.

*jwluo@semi.ac.cn

Silicon, CdTe, and III-V semiconductors are important materials in the photovoltaic industries because they are excellent light absorbers with high carrier mobilities, but their stabilities in aqueous solution are limited (<days) [5–7]. On the other hand, wide-band-gap oxides, such as TiO_2, $SrTiO_3$, and WO_3, are highly resistant to photocorrosion in aqueous solution, but they suffer from poor PEC performances because their band gaps are too wide to absorb a sufficient amount of the solar spectrum [1–5]. Thus far, no material capable of harvesting the whole visible-light spectrum with stability against photocorrosion has been found. Current knowledge is insufficient to identify semiconductor photocatalysts simultaneously possessing efficiency and stability. Thus, empirical approaches are often invoked with the hope of discovering effective photocatalysts, such as using high-throughput experimental [3] or computational [8,9] screening of numerous materials as solar water-splitting photocatalysts. In the end, hundreds of thousands of semiconducting compounds will likely be examined and tested for PEC efficiency and stability without any certainty of success. Chen and Wang [10] recently examined the stability of 30 photocatalytic semiconductors in aqueous solution using the method developed by H. Gerischer [11] in 1977 in combination with the first-principles calculations and discussed their thermodynamic stabilities and trends against oxidative and reductive photocorrosion. Whereas, the primary aim of this study is to address whether a semiconductor photocatalyst can be simultaneously efficient and stable and thereby shed light on the knowledge-based design of highly efficient PEC water-splitting cells.

Many of the most stable metal-oxide PEC photocatalysts possess wide band gaps because the width of the band gap is believed to be a measure of the chemical bond strength [1]. However, GaN and ZnS have even larger band gaps than stable TiO_2 and WO_3, but these semiconductors exhibit photodecomposition in aqueous solution [1,2,4,5]. The high-VB energy of both GaN and ZnS, where the VB edge consists of high-energy N 2*p* or S 2*p* orbitals, is a prominent feature distinguishing these semiconductors from TiO_2 and WO_3, where the VB edge is dominated by low-energy O 2*p* orbitals and stays low and somewhat stable at approximately 3.0 V vs NHE. Cu_2O is a rare metal oxide providing favorable energy positions and an optimal band gap for PEC water splitting resulting from a high VB, which is primarily composed of Cu 3*d* orbitals instead of O 2*p* orbitals, but Cu_2O is also unstable in aqueous solution [12]. Thus, we speculate that the energy position of the VB edge, rather than the width of the band gap, determines the stability of a semiconductor under illumination in aqueous solution: a more positive VB potential (lower energy) results in better thermodynamic stability. Because the CB potential must be negative vs NHE, a more positive VB potential indicates a wider band gap and hence less efficient PEC photocatalysis owing to less harvested sunlight. Therefore, a proper balance must be attained between the stability and efficiency of a semiconductor for PEC water splitting. To reveal the hidden relationship between the VB potential and the thermodynamic stability for semiconducting PEC photocatalysts, here, we examine 202 semiconductors that are known to either catalyze overall water splitting or reduce or oxidize water in the presence of an external sacrificial redox agent as collected in three comprehensive review articles [13–15]. Note that we do not have any bias in choosing the known catalytic materials in our study. We find that the desired photocorrosion stability sets a limit of the highest possible VB potential at 2.48 V vs NHE for semiconducting PEC photocatalysts, which, in turn, excludes PEC-photocatalytic materials with band gaps less than 2.48 eV. We also demonstrate that such a limitation has deep roots in the underlying physics after deducing the relation between the energy position of the VB edge and free energy of a semiconductor.

II. METHODS

A. Assessing the thermodynamic stabilities of semiconductors against photocorrosion

The thermodynamic stability of a semiconductor in contact with an electrolyte solution is characterized by the decomposition redox potentials, which are the required minimum Fermi energy of the electrons and holes driving the reductive- and oxidative-decomposition reactions, respectively [10,11]. By analyzing the relative positions of the competing potentials of water-redox reactions, semiconductor-decomposition reactions, and semiconductor band edges, we can determine the stabilities of the semiconductors in the PEC process [10,11]. For an optimized semiconductor exhibiting a band gap straddling both HER and OER potentials, Fig. 1(a) illustrates the thermodynamic stability requirement that the reductive-decomposition potential ϕ^{re} of a semiconductor must be more negative than the HER potential $\phi^0(H^+/H_2)$ for water reduction, where photogenerated electrons prefer to participate in water reduction to produce H_2, and that the oxidative decomposition potential ϕ^{ox} of a semiconductor must be more positive than the OER potential $\phi^0(H_2O/O_2)$ for water oxidation, where photogenerated holes prefer to participate in water oxidation to produce oxygen. [Note that Fig. 1(a) shows a case of semiconductor ϕ^{ox} being above its VB edge but below the $\phi^0(H_2O/O_2)$, which was assigned by Gerischer as metastable protected by solvent in his original paper [11]. This different assignment may lead to overestimation of the stability of semiconductor photocatalysts, but will not affect our conclusions as we will discuss below.] Otherwise, as shown in Figs. 1(b)–1(d), photogenerated electrons or holes prefer to drive the self-decomposition of the semiconductor instead of the water-redox reactions, resulting in instability under illumination in aqueous solution. In this case, a

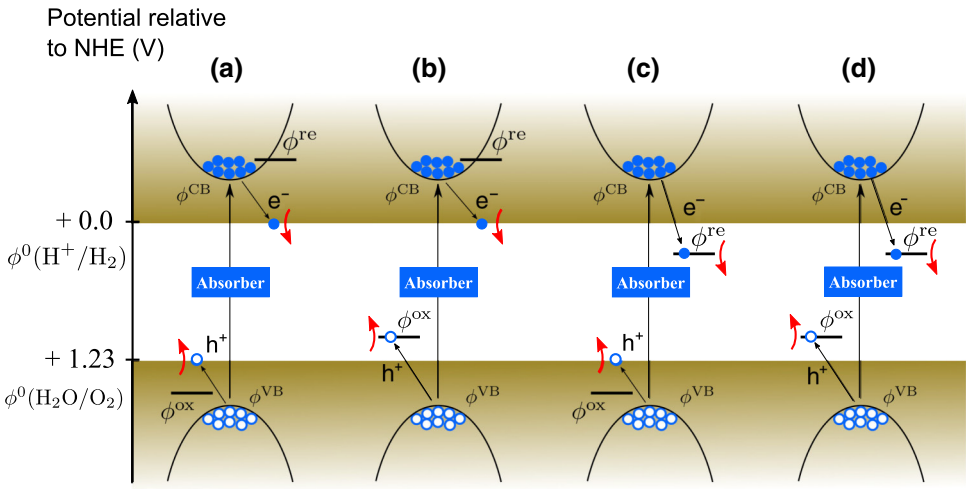

FIG. 1. Classification of the semiconductor decomposition-redox potentials with respect to the water-redox potentials. For optimized PEC water splitting, a semiconductor should possess a band gap straddling the HER and OER potentials. The relative energy positions between the band-edge energy, the water-redox potentials, and the semiconductor decomposition-redox potentials characterize the stability of the semiconductor against photocorrosion. (a) The semiconductor is stable against photocorrosion because of a more negative reductive-photodecomposition potential ϕ^{re} than the HER potential $\phi^0(H^+/H_2)$ and a more positive oxidative-photodecomposition potential ϕ^{ox} than the OER potential $\phi^0(H_2O/O_2)$. (b) The semiconductor is susceptible to oxidative photodecomposition because of the less positive oxidative-photodecomposition potential ϕ^{ox} than the OER potential $\phi^0(H_2O/O_2)$. (c) The semiconductor is susceptible to reductive photodecomposition because of the less negative reductive-photodecomposition potential ϕ^{re} than the HER potential $\phi^0(H^+/H_2)$. (d) The semiconductor is susceptible to both reductive and oxidative photodecompositions.

semiconductor has at least one oxidative-decomposition reaction at a potential ϕ^{ox} more negative than the OER potential $\phi^0(H_2O/O_2)$ [Figs. 1(b) and 1(d)] or at least one reductive-decomposition reaction at a potential ϕ^{re} more positive than the HER potential $\phi^0(H^+/H_2)$ [Figs. 1(c) and 1(d)]. Notably, a semiconductor exhibiting a band gap not straddling the HER and OER potentials could still be stable against photocorrosion, even if the relative positions between the decomposition-redox potentials and the water-redox potentials are similar, as shown in Figs. 1(b)–1(d). For instance, if the reductive-decomposition potential ϕ^{re} is more positive than the HER potential $\phi^0(H^+/H_2)$, but less positive than the CB potential ϕ^{CB}, photogenerated electrons prefer to stay at the CB edge instead of driving self-decomposition before recombination with holes.

III. RESULTS AND DISCUSSION

A. Validating the theoretical predictions

We can now assess the stability of semiconductors under solar water-splitting conditions using the criterion shown in Fig. 1 by determining the energy positions of the band edges and the redox-decomposition potentials with respect to the water-redox potentials for semiconductors. We examine 202 inorganic materials known to either catalyze overall water splitting or reduce or oxidize water in the presence of an external sacrificial redox agent [13–15]. We organize these 202 materials in Fig. 2 from left to right in descending order of energy of their VB-edge potentials (at pH = 0). The orange color marks the photocorrosion-resistant materials, and the blue color indicates the remaining unstable materials. Details of all the predicted lowest reductive and highest oxidative photodecomposition potentials and corresponding reactions are given in the Supplementary Materials [16] Table S1 [13,14,17–97]. We see that all semiconductors that are stable against photocorrosion are, as expected, oxides or halides with low VB energies.

To test these theoretical predictions, we perform detailed comparisons with experimental measurements for widely studied or recently reported semiconductor photocatalysts, such as TiO_2, Cu_2O, $BiVO_4$, Ag_3PO_4, β-Ge_3N_4, and BiOX (X = Cl, Br, and I).

Since the demonstration of PEC water splitting over TiO_2 by Fujishima and Honda [98], TiO_2 has been the most widely used oxide for photocatalytic applications owing to its low cost and long-term stability in aqueous solution [1–3,99]. Figure 3(a) shows that the predicted reductive-decomposition potential ϕ^{re} and oxidative-decomposition potential ϕ^{ox} straddle the HER potential $\phi^0(H^+/H_2)$ and OER potential $\phi^0(H_2O/O_2)$, indicating that TiO_2 is thermodynamically stable under water-splitting conditions, which is in excellent agreement with experiments. As an active photocatalyst under visible-light illumination, Cu_2O has recently attracted attention [12], even though

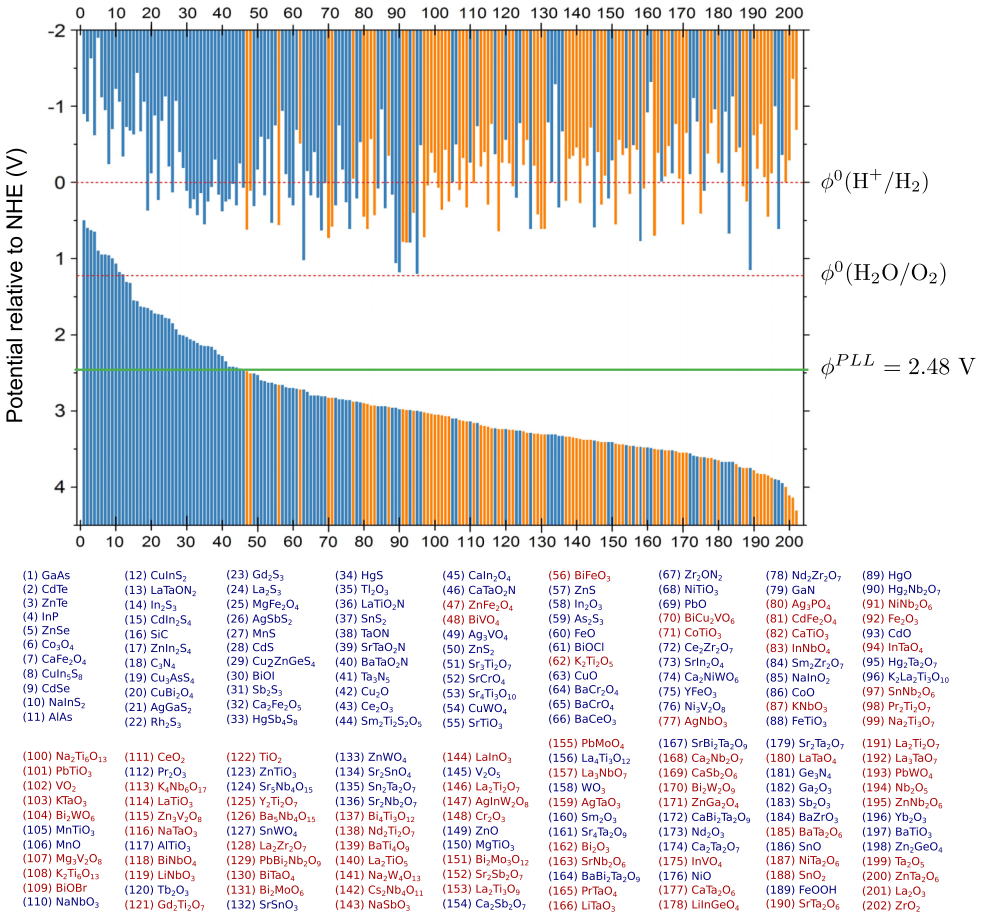

FIG. 2. Band alignments and stabilities of 202 semiconductors under water-splitting conditions. The stabilities of 202 inorganic materials known to either catalyze overall water splitting or reduce or oxidize water in the presence of an external sacrificial redox agent under water-splitting conditions are evaluated. Photocorrosion-resistant semiconductor photocatalysts are marked in the orange color, and the remaining unstable semiconductor photocatalysts are indicated by the blue color. These 202 materials are organized from left to right in descending order of energy of their VB-edge potentials (at pH = 0). The emergence of a photocatalyst line in the VB-edge potentials (analogous to the tree line on a mountain) is evident. Above this line, no semiconductor photocatalyst is stable against photocorrosion.

Cu_2O suffers from poor stability in aqueous solution. We predict that, as shown in Fig. 3(a), both the reductive and oxidative reactions decompose Cu_2O as a result of the more positive reductive-decomposition potential ϕ^{re} than the HER potential $\phi^0(H^+/H_2)$ and the much more negative oxidative-decomposition potential ϕ^{ox} than the OER potential $\phi^0(H_2O/O_2)$, in agreement with the previous experimental report [12]. Here, a slight difference is observed in which our predicted oxidative-decomposition potential ϕ^{ox} is higher than that determined in an earlier study [12], where both redox potentials lie within the band gap. In recent years, the visible-light-active $BiVO_4$ semiconductor has also been widely studied as a promising photoanode in water-splitting PEC cells [100]. Two opposite opinions have been reported on the stability of $BiVO_4$ against photocorrosion. Some experiments presented evidence suggesting the material is stable in PEC water splitting [101], whereas experimental evidence [102] has also been presented suggesting degradation occurs, as the photocurrent generated from the bare $BiVO_4$ film decreases significantly within a few minutes under illumination, ascribed to severe anodic photocorrosion occurring on the $BiVO_4$ surface. The observed remarkable reduction of the V/Bi ratio on the $BiVO_4$ surface under illumination was another supporting evidence for the photodecomposition of $BiVO_4$ [102]. Here, our prediction suggests that $BiVO_4$ is resistant to photocorrosion at pH = 0, as the oxidative decomposition potential ($\phi^{ox} = 1.36$ V vs NHE) is more positive than the OER potential $\phi^0(H_2O/O_2)$, and the potential of the CB edge is more positive than both the reductive decomposition potential ($\phi^{re} = 0.05$ V vs NHE) and HER potential $\phi^0(H^+/H_2)$; however, the reductive decomposition potential is more positive than the HER potential $\phi^0(H^+/H_2)$, implying that $BiVO_4$ may become unstable as the pH value increases. Ag_3PO_4, having a 2.4 eV band gap that absorbs visible light to oxidize water into oxygen [103,104], has been regarded as chemically stable in aqueous solution [104]. However, experiments [103] have also reported that Ag^+ transforms into Ag during the active photocatalytic process in the absence of an electron acceptor, resulting in black metallic-Ag particles accumulating on the Ag_3PO_4 surface, which suppresses further photocatalytic activity by preventing light absorption and thus indicates photodecomposition of Ag_3PO_4. Here, we predict that Ag_3PO_4 is stable against photocorrosion, as the CB-edge potential is lower than both the reductive-decomposition potential ϕ^{re} and the HER potential $\phi^0(H^+/H_2)$, and thus, the photogenerated electrons prefer to stay at the CB edge instead of driving HER or reductive photodecomposition; however, the

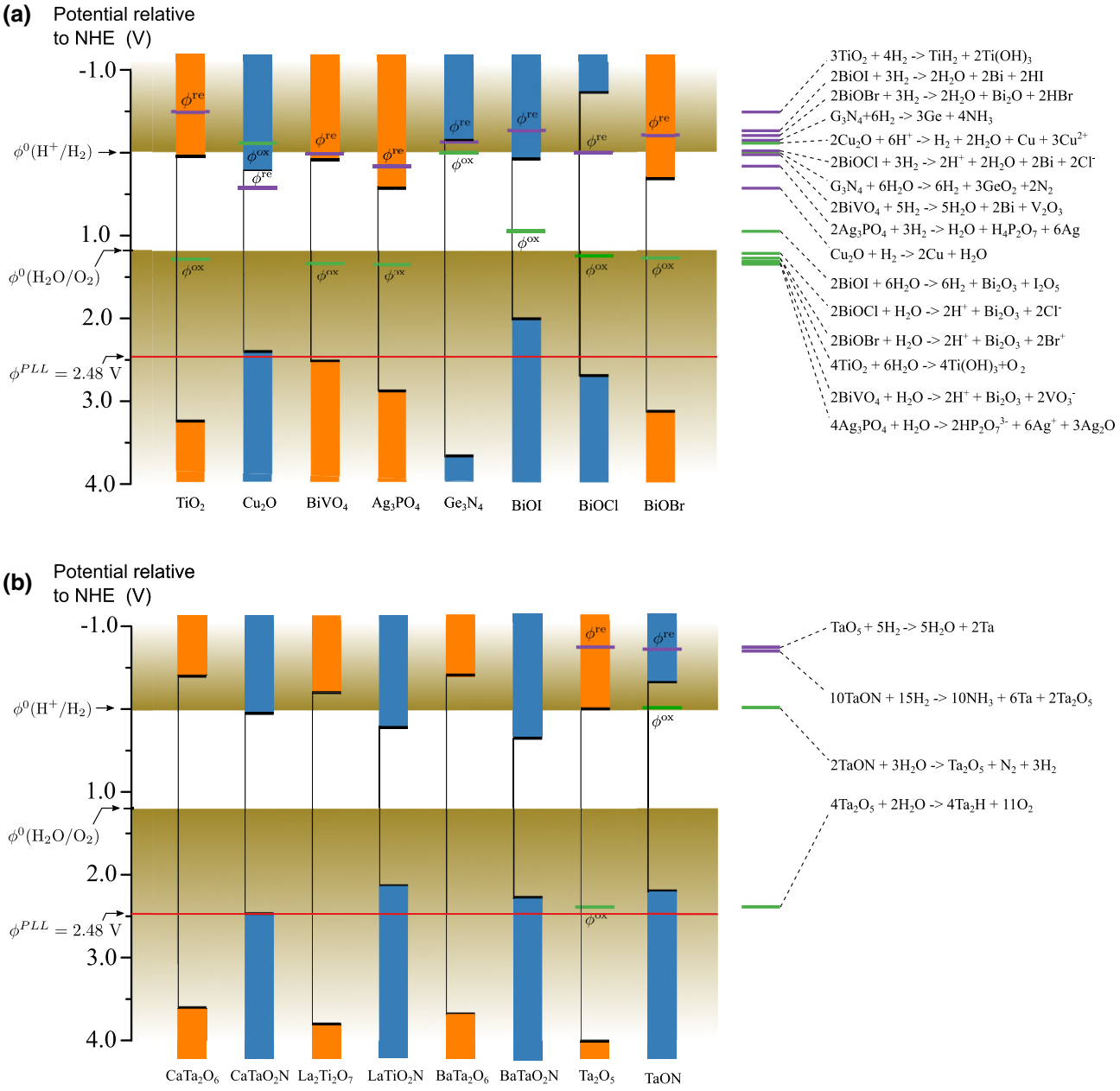

FIG. 3. Stability of various semiconductors and oxynitrides under solar water-splitting conditions. (a) The energy positions (vs NHE) of the CB and VB edges of various selected semiconductors, including anatase TiO_2, Cu_2O, $BiVO_4$, β-Ge_3N_4, and BiOX (X = I, Cl, or Br) at pH = 0, and the photodecomposition-redox potentials under solar water-splitting conditions. Photocorrosion-resistant semiconductor photocatalysts are marked in the orange color, and the remaining unstable semiconductor photocatalysts are indicated by the blue color. The corresponding photodecomposition-redox reactions of these semiconductors are listed on the right. (b) The energy positions of the CB and VB edges of various oxynitrides and their oxide counterparts.

lowest reductive-decomposition potential ($\phi^{re} = 0.19$ V vs NHE) of Ag_3PO_4 is more positive than the HER potential $\phi^0(H^+/H_2)$. Note that at a high pH value, Ag_3PO_4 becomes unstable because of a slightly more negative reductive-decomposition potential (at pH = 0) crossing the energy of the CB edge, as shown in Fig. 5(e), which explains the previously reported self-decomposition of Ag_3PO_4 [103].

RuO_2-loaded β-Ge_3N_4 was the first successful example of a nonoxide photocatalyst for overall water splitting [93]. Unfortunately, we find that β-Ge_3N_4 is unstable against photocorrosion. Figure 3(a) shows that the photodecomposition-oxidative potential of β-Ge_3N_4 is much more negative than the OER potential, indicating that photogenerated holes cause the self-decomposition of β-Ge_3N_4 with an oxidation reaction of $Ge_3N_4 + 6H_2O$

$\rightarrow 6H_2 + 3GeO_2 + 2N_2$. The photodecomposition of β-Ge_3N_4 was experimentally confirmed by the observation of a relatively high amount of N_2 evolution during water splitting [105]. Bismuth oxyhalides, BiOX (where X = Cl, Br or I), have recently been studied [17] as alternate nonoxide photocatalysts. A very recent experiment reported that BiOBr exhibited excellent stability in aqueous solution, but both BiOI and BiOCl possessed poor stabilities [106]. These experimental results are consistent with our predictions since BiOBr is predicted to be photocorrosion resistant, as the two photodecomposition-redox potentials ($\phi^{re} = -0.18$ V, $\phi^{ox} = 1.32$ V vs NHE) of BiOBr straddle the HER and OER potentials; whereas, BiOI is susceptible to oxidative photodecomposition, as indicated by the more negative oxidation potential ($\phi^{ox} = 0.96$ V) than the OER potential [$\phi^0(H_2O/O_2) = 1.23$ V vs NHE], and BiOCl is subject to reductive photodecomposition because of the slightly more positive reductive potential of $\phi^{re} = 0.04$ V vs NHE.

B. Photocorrosion-induced limit for the VB potentials of photocatalysts

Figure 2 indicates that the semiconductors near the left side of the plot are all unstable (marked in blue), whereas most of the stable semiconductors (marked in orange) reside on the right side of the plot. Surprisingly, we observe a line at 2.48 V vs NHE in the VB-edge potentials, above which no semiconductor photocatalysts are stable against photocorrosion. The emergence of such a limiting line for the photocatalyst-VB potential indicates that the photocorrosion sets a limit for the highest possible VB-edge potential for a stable semiconductor photocatalyst. We call this limiting line the photocatalyst-limiting line (or PLL, $\phi^{PLL} = 2.48$ V vs NHE). Although semiconductors with VB-edge potentials below this PLL are not necessarily stable against photocorrosion, a VB-edge potential below the PLL is required for a semiconductor photocatalyst to exhibit photocorrosion resistance. The overpotential between the PLL ($\phi^{PLL} = 2.48$ V) and the OER potential [$\phi^0(H_2O/O_2) = 1.23$ V vs NHE] poses a major challenge for the development of high-performance photocatalyst materials. Because the potential of the CB edge must be more negative than the HER potential $\phi^0(H^+/H_2)$, the limit for photocorrosion-resistant photocatalysts with the highest VB potential at 2.48 V excludes PEC photocatalytic materials with band gaps less than 2.48 eV.

As shown in Fig. 2, photocorrosion-resistant semiconductors always possess wide band gaps, and therefore, suffer from poor PEC activity under visible light. Several strategies have emerged to overcome this limitation, such as incorporating nitrogen into the metal-oxide lattice to form oxynitrides [107,108], which decreases the band gap by raising the VB, as the N *2p* orbital is higher in energy than the O *2p* orbital. Figure 3(b) shows that the energy positions of the VB edges of all the examined oxynitrides are remarkably raised relative to the VB edges of their oxide counterparts (even passing over the PLL), whereas their CB edges show little change in energy. However, all these oxynitrides are predicted to be unstable, consistent with the manifestation of the PLL, but their oxide counterparts are stable against photocorrosion. For example, the oxidative-decomposition potential of TaON is $\phi^{ox} = 0.06$ V vs NHE for the oxidative reaction of $2TaON + 3H_2O \rightarrow 3H_2 + N_2 + Ta_2O_5$, indicating that TaON will decompose back to the more stable oxide Ta_2O_5 under water-splitting conditions. This prediction was confirmed by experimental observations [107,108], where a low level of N_2 evolution during solar water splitting was observed over this photoelectrode in the initial stages, which was attributed to the partial decomposition of the oxynitride driven by photogenerated holes. In such a self-decomposition progress, a Ta_2O_5 thin film is built up on top of TaON to serve as an oxide protection layer to suppress the further decomposition of TaON, which explains the experimentally observed ceasing of N_2 evolution after the initial stages. Because photogenerated holes are difficult to extract across a newly formed oxide protection layer to drive OER, a low quantum yield (5%–6%) for solar water splitting [108] is thus expected using an oxynitride as a photocatalyst.

The introduction of defects is another attractive method to raise the VB of photocorrosion-resistant oxides. For instance, introducing disorder through hydrogenation in the surface layers of nanophase TiO_2 has been examined to extend the absorption edge into the visible-light region [109,110]. The modified TiO_2 (called black TiO_2) exhibited activity under visible light. However, experiments also reported that the H_2 production rate dropped by two orders of magnitude when black TiO_2 was illuminated with visible and infrared light, with incident light of wavelengths shorter than 400 nm filtered out [109,111]. This observation may be due to the coating of black TiO_2 by a layer of wide-band-gap white TiO_2, which functions as an oxide protection layer to suppress further degradation, but also blocks photogenerated carriers to drive HER and OER. This speculation is supported by the experimental observation [109] of identical Ti 2p X-ray photoelectron spectroscopy (XPS) spectra for both white and black TiO_2. The coating of the white TiO_2 layer could stem from the decomposition of black TiO_2, which was revealed to have a nanocrystalline-TiO_2 core and a highly disordered hydrogen-doped TiO_2 shell (ca. 1-nm thick) [111].

We conclude that, although we can modify a photocorrosion-resistant metal oxide to raise the VB edge to extend the band gap into the visible-light region, the modified metal oxide typically becomes unstable because of the VB edge approaching the PLL, implying that the PLL ($\phi^{PLL} = 2.48$ V vs NHE) is universal for PEC-semiconducting photocatalysts. Notice that in practical

PEC cells, catalysts are additionally deposited on semiconductor surfaces to promote the OER and HER reactions by lowering their respective overpotentials. These catalysts may slow down the photodecomposition rate of the decorated semiconductor, but will not fully protect it since they can absorb sunlight and thus have to avoid to fully cover the surface of the semiconductor photocatalyst. Here, we can safely neglect the catalyst effect on stability [8–10,112].

C. Revisiting the upper-bound efficiency of single-band-gap PEC water splitting

The absorbed photon flux J_g (photons $s^{-1}\,m^{-2}$) is an important quantity in solar-efficiency calculations and is defined as $J_g = \int_{E_g}^{\infty} J_{\hbar\upsilon}\alpha_{\hbar\upsilon} d\hbar\upsilon$, where $J_{\hbar\upsilon}$ is the air mass (AM)1.5 global-solar spectrum as shown in Fig. 4(a). To evaluate the theoretical limiting efficiency, we make a common assumption that complete absorption ($\alpha_{\hbar\upsilon} = 1$) of all photons above the band gap of the semiconductor takes place [113,114]. Figure 4(b) shows the maximum harvested solar-energy percentage $P = J_g / \int_0^{\infty} J_{\hbar\upsilon} d\hbar\upsilon$ for a semiconductor with band gap E_g. A semiconductor with a 2.48-eV band gap can only absorb a small part of the solar spectrum ($E_{\text{phtoton}} \geq 2.48$ eV), accounting for approximately 23% of solar radiation, as shown in Fig. 4(b), and possessing a maximum achievable efficiency of 13% for a single-band-gap photovoltaic cell according to the Shockley-Queisser limit [115]. However, for solar water-splitting applications, the maximum achievable STH efficiency is further reduced to 7.8% [113,114] as shown in Fig. 4 (or 7.1% for a realistic single-junction PEC cell [114]) because only 1.23 eV, rather than 2.48 eV, per absorbed photon is converted to chemical energy through driving the overall water-splitting reaction. Therefore, the required PEC stability remarkably decreases the STH-limiting efficiency of single-band-gap PEC water splitting from the previously thought value of 30.7% to 7.8%, which is even lower than the 10% efficiency required for commercial applications [1,3]. This finding emphasizes the difficulty of finding a stable semiconducting photocatalyst with a high-PEC efficiency even after an extensive search over half a century for materials that simultaneously meet the requirements of both favorable energy-band positions and photocorrosion resistance. In the above discussion, we ignore the effect of OER and HER overpotentials, which will further lower the predicted 7.8% upper-bound efficiency of PEC water splitting.

D. The physics underlying the photocorrosion-induced limit of the VB potentials for photocatalysts

To uncover the underlying physics, we attempt to derive the relation between the VB potential and free energy for semiconducting photocatalysts considering that the photocorrosion resistance of a semiconducting photocatalyst is highly coupled to the Gibbs free energy of formation. A semiconducting photocatalyst that possesses a more negative Gibbs free energy of formation requires more free energy supplied from photogenerated carriers to drive the decomposition-redox reactions, and hence is more likely to be stable against photocorrosion. For example, the Gibbs free energy of formation of M_aX_b can be written as $\Delta_f G(M_aX_b) = \Delta_f H(M_aX_b) - TS$ (T is the temperature; S is the entropy), and the enthalpy of formation is defined as $\Delta_f H(M_aX_b) = E_{\text{tot}}(M_aX_b) - a\mu_M - b\mu_X$ [μ_i is the chemical potential of element i; $E_{\text{tot}}(M_aX_b)$ is the total energy of M_aX_b]. The enthalpy of formation $\Delta_f H(M_aX_b)$

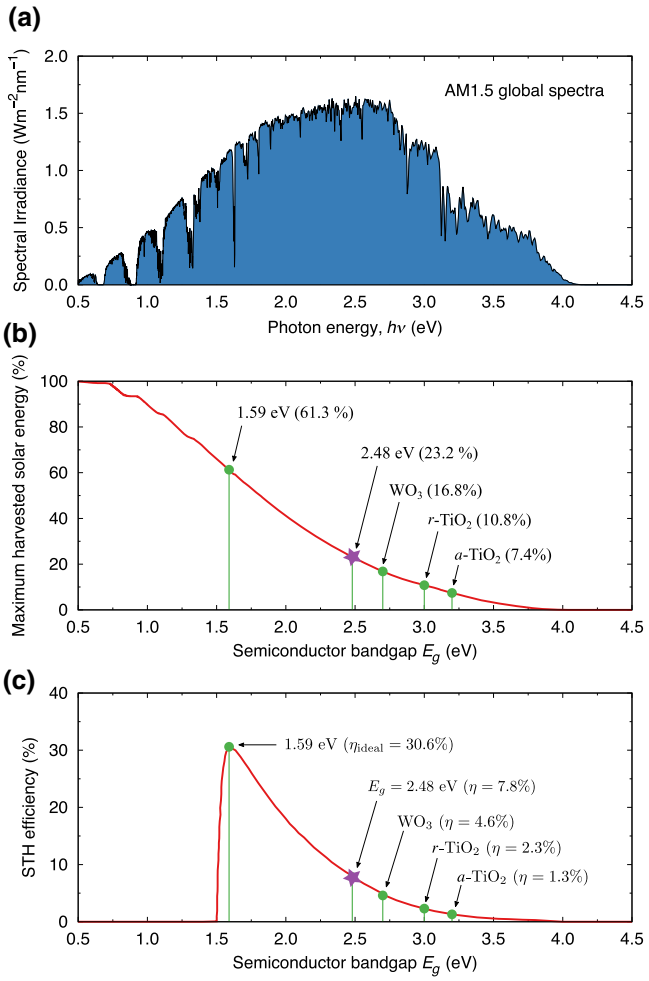

FIG. 4. Limiting STH efficiency vs the semiconductor band gap (E_g) for single-absorber PEC cells. (A) Solar spectral distribution based on AM1.5 global data. (B) Maximum harvested solar-energy percentage of semiconductor absorbers vs the semiconductor band gap E_g. The values corresponding to the optimal band gap (1.59 eV), the photocorrosion-limited smallest band gap (2.48 eV), WO_3, rutile TiO_2, and anatase TiO_2 are also indicated. (C) The maximum STH efficiencies of the single-absorber PEC cells for the ideal case without considering stability ($E_g = 1.59$ eV, $\eta = 30.6\%$), for the ideal case considering the photocorrosion restriction ($E_g = 2.48$ eV, $\eta = 7.8\%$), and for the cases of WO_3, rutile TiO_2, and anatase TiO_2 cells.

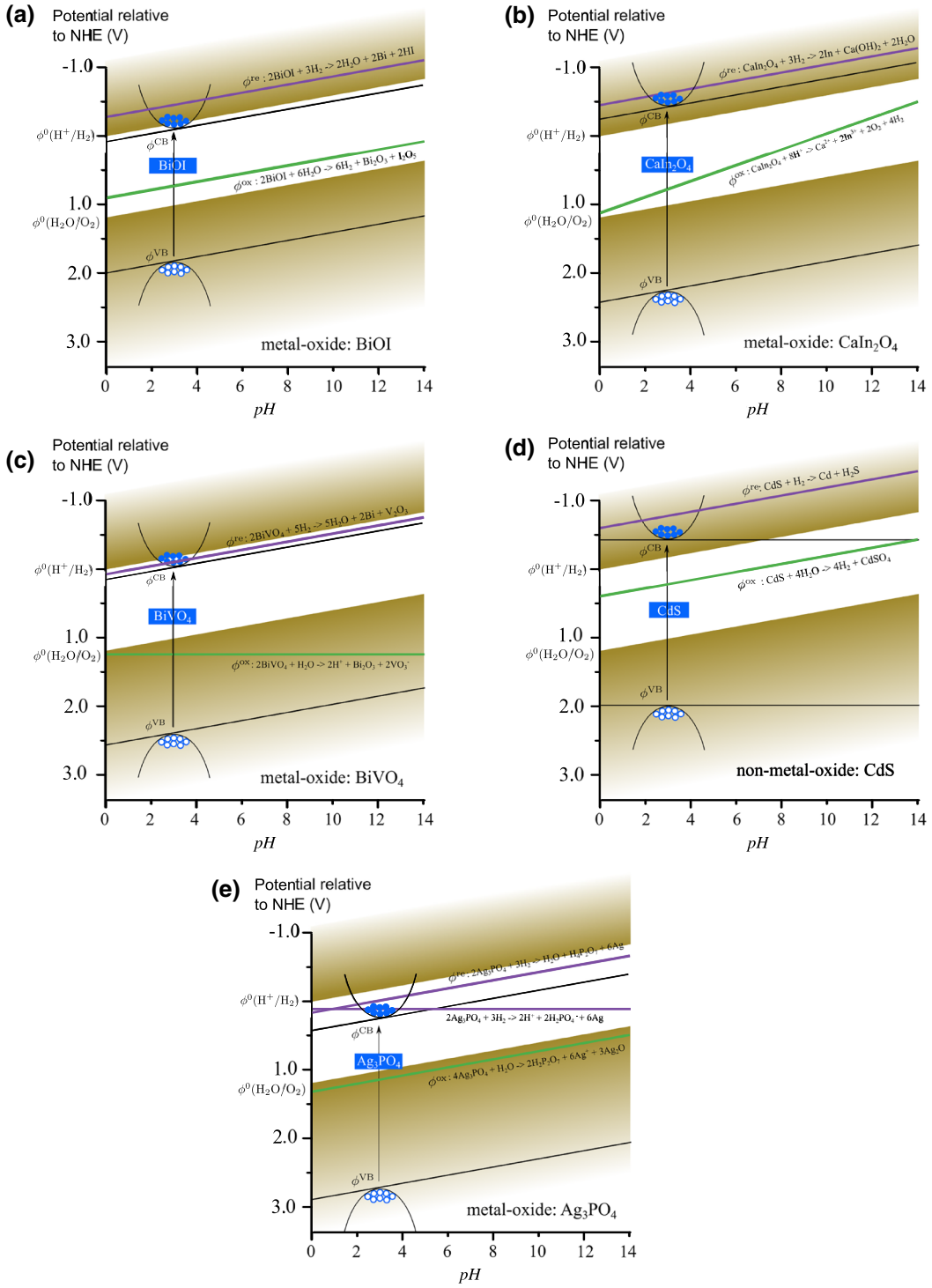

FIG. 5. pH dependences of the photodecomposition-redox potentials, the CB and VB edges of photocatalysts, and the water-redox potentials. (a) In metal oxides such as BiOI, both the photodecomposition-reductive and -oxidative reactions do not explicitly involve H^+ or OH^-, so they follow the Nernstian relation with a slope of -0.059 V/pH, the same as the band edges as well as water-redox potentials. (b) In metal oxides such as $CaIn_2O_2$, the photodecomposition-oxidative reaction explicitly involves H^+ on the left-hand side, so the oxidation-redox potential vs pH value has a larger slope than that of $\phi^0(H^+/H_2)$ vs pH. (c) In metal oxides such as $BiVO_4$, the photodecomposition-oxidative reaction explicitly involves H^+ on the right-hand side, so the oxidation-redox potential vs pH value has a smaller slope than that of $\phi^0(H^+/H_2)$ vs pH. (d) In nonmetal-oxide CdS, the CB and VB edges are fixed to values at pH = 0. (e) In metal-oxide Ag_3PO_4, both the lowest photodecomposition reductive and highest oxidative reactions do not explicitly involve H^+ or OH^-, but the second photodecomposition-reductive reaction explicitly contains H^+ on the right-hand side and is independent of the pH value. At a high pH value, this reductive reaction is crossed over with the CB edge, making Ag_3PO_4 unstable.

is highly correlated to the VB energy in which a lower VB energy results in a more negative $\Delta_f H(M_aX_b)$ for a semiconductor. Because the VB-edge states are generally the anion atom-centered bonding states, a lower VB indicates either a stronger covalent bond or a larger Coulomb binding between anions and cations, which, in turn, results in a more negative total energy $E_{\rm tot}(M_aX_b)$ (and $\Delta_f H$) for the semiconductor. Furthermore, combining the $E_{\rm VB}$ vs E_g relationship proposed by Butler and Ginley [116] and the E_g vs $\Delta_f H$ relationship proposed by Portier *et al.* [117], we can obtain a quantitative relationship between $E_{\rm VB}$ and $\Delta_f H$ for a semiconductor M_aX_b at pH = 0:

$$E_{\rm VB} = 0.619\ \chi(M_aX_b) + 0.5\ A_c \exp(-2.95 \times 10^{-5} \times \Delta_f H/n_e) - 1.942, \quad (1)$$

where $\chi(M_aX_b) = (\chi_M^a \times \chi_X^b)^{1/(a+b)}$, χ_M^a and χ_X^b are the absolute electronegativities of atoms M and X, respectively, n_e is the number of electrons involved in the reaction, A_c is a property of the cation, and $E_{\rm VB}$ and $\Delta_f H$ are in eV (see the Appendix D and E for more details).

Based on the deduced $E_{\rm VB}$ vs $\Delta_f H$ relationship, we can verify the photocorrosion-induced limit of the VB potentials by artificially raising the VB-edge potentials of all the stable semiconducting photocatalysts to 2.48 V vs NHE and adjusting $\Delta_f H$ according to Eq. (1). In this case, we find that all the semiconductors again become unstable. For example, the VB-edge potential of TiO_2 is at 3.25 V vs NHE, and the Gibbs free energy is −888.8 kJ/mol with the predicted reductive- and oxidative-photodecomposition potentials of $\phi^{\rm re} = -0.53$ V and $\phi^{\rm ox} = 1.30$ V, respectively (corresponding reactions are given in Table S1 [13,14,16–97]). If we artificially raise the VB-edge potential from 3.25 to 2.48 V vs NHE, the Gibbs free energy changes from −888.8 to −801.50 kJ/mol according to Eq. (1), and TiO_2 becomes unstable, as the modified reductive-photodecomposition potential ($\phi^{\rm re} = 0.78$ V) becomes more positive than the HER potential. If we upshift the VB-edge potential of Bi_2WO_6 from 3.27 to 2.48 V, the Gibbs free energy changes from −1708.34 to −1439.69 kJ/mol, and the reductive- and oxidative-photodecomposition potentials change from $\phi^{\rm re} = -0.25$ to 0.07 V and from $\phi^{\rm ox} = 1.28$ to 0.28 V, respectively. Subsequently, Bi_2WO_6 again becomes unstable upon upshifting the VB potential above the PLL. Thereby, we illustrate that the photocorrosion-induced limit of the VB potentials for photocatalysts has a deep root in the underlying physics.

IV. CONCLUSIONS

We revealed that thermodynamic stability is strongly coupled to the energy position of the VB edge for semiconducting PEC photocatalysts, setting limits for the highest possible VB-edge potential at 2.48 V vs NHE (called the PLL) and for the minimum possible band gap at 2.48 eV. These limits remarkably reduce the STH limiting efficiency for single-band-gap PEC water splitting from the commonly believed 30.7% to approximately 8%, even lower than the 10% efficiency required for commercial applications [1–3]. Although this conclusion was drawn from data at pH = 0, the limits are also applicable in a finite pH range (see discussion on pH dependence in Appendix F). Because the predicted limiting STH efficiency is too low, future efforts toward attaining highly efficient PEC solar water splitting must shift from searching for PEC photocatalysts to strategies that decouple the thermodynamic stability and PEC efficiency. For example, metal-oxide protection layers have been used to stabilize narrow-band-gap (PEC-active) semiconducting photocatalysts, such as Cu_2O [12], Si [6,118,119], CdTe [119], and III-V [7] semiconductors as well as some modified oxides. For this purpose, the focus should shift toward interface engineering for the simultaneous optimization of the built-in field, interface quality, and carrier extraction to maximize the photovoltage of an oxide-protected water-splitting photocatalyst [112,118,120,121]. Furthermore, a dual-band-gap Z-scheme water-splitting system using two different semiconducting photocatalysts could also overcome the predicted 8% limiting STH efficiency if the photoanode is resistant to photoanodic decomposition and if the photocathode is resistant to photocathodic decomposition.

ACKNOWLEDGMENTS

We thank S. Chen for helpful discussion and carefully reading the manuscript. J.W.L thanks A. Zunger for helpful discussions. J.W.L. was supported by the National Natural Science Foundation of China (NSFC) under Grants No. 61474116 and No. 61811530022 and the National Young 1000 Talents Plan. L.J.G was supported by NSFC under Grant No. 11404074. S.H.W. was supported by the NSFC under Grants No. U1530401 and No. 51672023 and the National Key Research and Development Program of China under Grant No. 2016YFB0700700.

APPENDIX A: PREDICTING THE DECOMPOSITION-REDOX POTENTIALS OF SEMICONDUCTORS

We can reasonably estimate the decomposition reductive and oxidative potentials ($\phi^{\rm re}$ and $\phi^{\rm ox}$) of semiconductors as the required minimum Fermi energies of electrons and holes to drive the reductive- and oxidative-decomposition reactions, respectively, since the electronic reactants are electrons in the reductive reactions and holes in the oxidative reactions. Gerischer [11,122] and Bard and Wrighton [123] have developed a thermodynamic approach for determining thermodynamic decomposition potentials of semiconductors in contact

with electrolytes. Taking a binary compound semiconductor MX (e.g., $M = \mathrm{Zn}$, Cd and $X = \mathrm{O}$, S, Se, Te) as an example, we use this approach to predict ϕ^{re} and ϕ^{ox} relative to NHE from the standard Gibbs free-energy changes $\Delta_{\mathrm{re}}G^0$ and $\Delta_{\mathrm{ox}}G^0$ of the reductive and oxidative full reactions, respectively: $\phi^{\mathrm{re}} = \Delta_{\mathrm{re}}G^0/zF + \phi(\mathrm{H}^+/\mathrm{H}_2)$ and $\phi^{\mathrm{ox}} = -\Delta_{\mathrm{ox}}G^0/zF + \phi(\mathrm{H}^+/\mathrm{H}_2)$. Here, Z is the oxidation state of metal M, F is the Faraday constant (1 Faraday = 96 500 Coulombs), $\Delta_{\mathrm{re}}G^0[= \Delta_f G^0_{MX} + (Z/2)\Delta_f G^0_{\mathrm{H}_2} - \Delta_f G^0_M - \Delta_f G^0_{X^{z-}} - z\Delta_f G^0_{\mathrm{H}^+}]$ is the standard Gibbs free-energy change of the reductive full reaction $MX + (Z/2)\mathrm{H}_2 + \mathrm{solv} \rightarrow M + X^{z-} \cdot \mathrm{solv} + z\mathrm{H}^+ \cdot \mathrm{solv}$, and $\Delta_{\mathrm{ox}}G^0[= \Delta_f G^0_{MX} + z\Delta_f G^0_{\mathrm{H}^+} - \Delta_f G^0_{M^{z+}} - \Delta_f G^0_X - (Z/2)\Delta_f G^0_{\mathrm{H}_2}]$ is the standard Gibbs free-energy change of the oxidative full reaction $MX + z\mathrm{H}^+ \cdot \mathrm{solv} \rightarrow M^{z+} \cdot \mathrm{solv} + X + (Z/2)\mathrm{H}_2$. Such predicted reductive- and oxidative-decomposition potentials of semiconductors are potentials at pH = 0 because they are relative to the NHE potential, which is $\phi(\mathrm{H}^+/\mathrm{H}_2) = 0$ at pH = 0.

APPENDIX B: DETERMINING THE ENERGY POSITIONS OF SEMICONDUCTOR BAND EDGES

We can determine the energy positions of semiconductor band edges (another key property to assess the thermodynamic stability) from a variety of experimental and theoretical techniques, such as x-ray and ultraviolet photoelectron spectroscopy (XPS and UPS) [124,125] and the flat band potential measurement using various (photo)electrochemical techniques [13,126]. Unfortunately, the energy uncertainty of the band edges determined by different techniques for a semiconductor is as large as 0.5 eV [124], owing to divergent dipole fields occurring in heterojunction interfaces when it is measured with different techniques. We, therefore, prefer to use the band edges of the compounds obtained from flat band potential measurement in aqueous solution, in which the semiconductor photocatalysts are in contact with electrolyte solution where the band position of the semiconductor is influenced by the interface of the semiconductor-liquid. If there is no available flat band potential data reported in literature for a semiconductor, we complement it by utilizing empirical calculations from the electronegativities of constitute elements as originally proposed by Butler and Ginley [116] for semiconductors.

APPENDIX C: FIRST-PRINCIPLES PREDICTION OF THE GIBBS FREE ENERGY FOR SEMICONDUCTORS WITH UNAVAILABLE DATA

We prefer to use the recommended values of the standard Gibbs free energy of formation $\Delta_f G$ for those compounds available in the CRC Handbook of Chemistry and Physics [127] and Lange's Handbook of Chemistry [128]. When the recommended value is not available for a solid compound, we approximate the standard Gibbs free energy of formation $\Delta_f G$ as the enthalpy of formation $\Delta_f H$ predicted from the first-principles density functional theory (DFT) based on the assumption that cells are operations under temperature 0 K since $\Delta_f G = \Delta_f H - T\Delta S$. The enthalpy of formation for a solid compound $\mathrm{M_aX_b}$ is defined as $\Delta_f H = E_{\mathrm{tot}}(M_aX_b) - a\mu_M - b\mu_X$, where $E_{\mathrm{tot}}(M_aX_b)$ is the total energy per formula unit of M_aX_b, and μ_M and μ_X are the total energies per atom of the elements M and X in their elemental reference phase. We can accurately predict all these total energies from the DFT calculations. Recently, Stevanović *et al*. [129] made a significant improvement of the calculation accuracy of the enthalpy of formation for solid compounds by adding a fitted correction to each DFT-predicted element chemical potential μ_i, termed as the fitted elemental-phase reference energies (FERE). By examining an extensive test set of solid compounds with the available measured $\Delta_f H$ values, the mean absolute error of reproduced $\Delta_f H$ is found to be remarkably reduced from 0.250 eV/atom (resulting from pure DFT calculations) to 0.054 eV/atom. Following Stevanović *et al*. [129], we utilize the VASP code to determine the $\Delta_f H$ of solid compounds without available values in the handbook using the all electron-projected augmented plane waves (PAW) method with Perdew-Burke-Ernzerhof (PBE) generalized gradient approximation (GGA) exchange-correlation functional. We use a plane-wave cut-off energy of at least 30% larger than the largest specified in the pseudopotentials used and a dense k-point mesh to achieve the total energy convergence of less than 3 meV/atom for a specific compound. An on-site Hubbard U term of $U = 3$ eV is adopted for d-orbitals of transition metal elements, except Cu and Ag ($U = 5$ eV) and Zn, Cd, and Hg ($U = 0$ eV). More details can be found in Ref. [129]. Note that at 0 K temperature, the entropy component ($-T\Delta S$) of the Gibbs free energy is zero, and therefore, $\Delta_f G = \Delta_f H$, whereas, in the standard state at 298.15 K, the entropy component, which is small in solid compounds and neglected in the first-principles calculations, makes the Gibbs free energy slightly more positive than the enthalpy of formation. We may predict some unstable compounds as stable and thus the predicted upper bound of the PEC efficiency is even lower in practice. Therefore, such potential error due to neglecting the entropy component will not change our conclusions in this work.

APPENDIX D: PREDICTION OF BAND-EDGE POSITIONS FOR SEMICONDUCTORS WITH UNAVAILABLE DATA

Although a number of methods have been used to determine the band-edge position of semiconductors, we favor the data obtained from flat band potential measurement in aqueous solution considering that the redox reactions

of the solar water splitting occur on a semiconductor-electrolyte interface in a similar condition. However, there are no available flat band potential data for some newly investigated semiconductors. We use the well-established empirical formula developed by Bulter and Ginley [116] to estimate the band-edge positions for those semiconductors. Bulter and Ginley [116] found that band-edge positions (with respect to the vacuum) at the semiconductor-electrolyte interface depend on the semiconductor electronegativity $\chi(M_aX_b) = (\chi_M^a \cdot \chi_X^b)^{1/(a+b)}$ (χ_M^a and χ_X^b are the absolute electronegativities of atoms M and X), and varies with pH following a linear relation known as the Nernstian relation [13]. According to this approach, the CB-edge position of a M_aX_b compound is

$$E_{\mathrm{CB}}(\mathrm{pH}) = \chi(M_aX_b) - 0.5E_g - E_0 + 0.059(\mathrm{pH}_{\mathrm{PZZP}} - \mathrm{pH}), \tag{D1}$$

where E_g is the semiconductor band gap, E_0 is the standard redox potential of the aqueous redox couple with respect to the NHE (the Fermi level of NHE at 25 °C is −4.5 eV with respect to the vacuum level), $\mathrm{pH}_{\mathrm{PZZP}}$ is the pH value at the point of zero zeta potential (PZZP) of the semiconductor, and the last term is the Nernstian relation. The $\mathrm{pH}_{\mathrm{PZZP}}$ can be estimated from $\chi(M_aX_b)$ with the following equation:

$$0.155\mathrm{pH}_{\mathrm{PZZP}} = 6.72 - \chi(M_aX_b). \tag{D2}$$

APPENDIX E: RELATIONSHIP BETWEEN THE VBM LEVEL AND STABILITY OF SEMICONDUCTOR MATERIALS

Here, we uncover the hidden relationship between the energy level of the VB edge and the stability (or the Gibbs free energy) for semiconductors. Comparing Eq. (1) and Eq. (D1), we obtain an expression for the energy position of the CB edge of the semiconductor at pH = 0:

$$E_{\mathrm{CB}}(\mathrm{pH}=0) = 0.619\chi(M_aX_b) - 0.5E_g - E_0 + 2.558. \tag{E1}$$

Because $E_{\mathrm{VB}} - E_{\mathrm{CB}} = E_g$, we obtain an expression for the VB-edge level:

$$E_{\mathrm{VB}}(\mathrm{pH}=0) = 0.619\chi(M_aX_b) + 0.5E_g - E_0 + 2.558. \tag{E2}$$

On the other hand, Portier *et al.* [117,130] found that the band gap E_g is a function of the entropy of formation $\Delta_f H$ for a semiconductor:

$$E_g = Ae^{(0.34\times E_{\Delta H^\circ})}, \tag{E3}$$

and

$$E_{\Delta H^\circ} = \frac{-5.224\times 10^{19}\times \Delta H^\circ}{N\times n_e}, \tag{E4}$$

where ΔH° is the standard enthalpy of formation of solid compounds in cal/mol, $N = 6.02\times 10^{23}$ is Avogadro's number, n_e is number of electrons involved in the formation reaction, and A_c is a property of the cation ($A_c = 0.8$, 1.35, and 1.0 for s-block, p-block, and d-block elements, respectively). Comparing Eq. (E3) and Eq. (E4), we obtain following expression:

$$E_g = A\times \exp\left(-\frac{2.95\times 10^{-5}}{n_e}\times \Delta H^\circ\right). \tag{E5}$$

Substituting this into Eq. (E2), we obtain an expression of the VB-edge position,

$$E_{\mathrm{VB}}(\mathrm{pH}=0) = 0.619\times\chi(M_aX_b) + 0.5A \times \exp\left(-\frac{2.95\times 10^{-5}}{n_e}\times \Delta H^\circ\right) + 2.558 - E_0 \tag{E6}$$

If the NHE is chosen as the reference electrode, E_0 is then 4.5 eV and substituted into Eq. (E6) yields

$$E_{\mathrm{VB}}(\mathrm{pH}=0) = 0.619\times\chi(M_aX_b) + 0.5A \times \exp\left(-\frac{2.95\times 10^{-5}}{n_e}\times \Delta H^\circ\right) - 1.942. \tag{E7}$$

APPENDIX F: pH DEPENDENCE OF SEMICONDUCTOR PHOTODECOMPOSITION POTENTIALS

The water redox potentials $\phi^0(\mathrm{O_2/H_2O})$ and $\phi^0(\mathrm{H^+/H_2})$ vary linearly with the pH value following the Nernstian relation [13], that is they change by −0.059 V/pH at 298 K and 1 atm. For semiconducting metal oxides, the potentials of both CB and VB edges vary with pH following the same Nernstian relation as the water redox potentials, as shown in Fig. 5. For nonmetal oxides, such as metal-sulfide semiconductors, the pH dependence of band-edge potentials appears more complicated than that for metal oxides, and has not been as thoroughly studied [13,116]. Here, we simply speculate the band-edge potentials of nonmetal oxides to be independent of the pH value, such as for CdS as shown in Fig. 5(d), since it will not change our conclusions drawn at pH = 0 as discussed below.

The pH dependence of photodecomposition-redox potentials for semiconducting photocatalysts depends on the reactants and products of the associated reactions [131]. Keeping in mind that the predicted ϕ^{re} and ϕ^{ox} are defined relative to $\phi^0(\mathrm{H^+/H_2})$, we classify photodecomposition-redox reactions following the simplified procedure for constructing Pourbaix diagrams [131] into three types: (1) A photodecomposition reaction that

does not explicitly involve hydrogen ions (H^+ or OH^-) gives a straight line parallel to the pH dependence of $\phi^0(H^+/H_2)$, such as both photodecomposition-reductive and -oxidative reactions of BiOI as shown in Fig. 5(a); (2) A reaction explicitly involving H^+ on the left-hand side (reactants) will give a straight line with a slope equal to $-0.059(1+h/n)$ V/pH, where h is the coefficient of H^+ and n is the number of free electrons, such as the photodecomposition-oxidative reaction of $CaIn_2O_4$ as shown in Fig. 5(b), where $h=8$ and $n=2$; (3) A reaction again explicitly involving H^+, but on the right-hand side the products will give a straight line with a slope equal to $-0.059(1\text{-}h/n)$ V/pH, such as the photodecomposition-oxidative reaction of $BiVO_4$ as shown in Fig. 5(c), with $h=2$ and $n=2$, and the second photodecomposition-reductive reaction of Ag_3PO_4 as shown in Fig. 5(e), with $h=2$ and $n=2$.

The stability of a semiconducting photocatalyst will not change if pH-dependent lines of the photodecomposition-redox potentials and band-edge potentials are parallel to the water-redox potentials, as shown in Fig. 5(a) for BiOI. The emergence of a crossover between band edges, photodecomposition-redox potentials, and/or water redox potentials with varying pH values may indicate a change of the stability of semiconducting photocatalysts as a function of pH values. However, as shown in Fig. 5, all four examined semiconducting photocatalysts do not incur changes of stability when the pH value changes. Nevertheless, $BiVO_4$ becomes more stable [Fig. 5(c)] but $CaIn_2O_4$ becomes less stable [Fig. 5(b)] and Ag_3PO_4 even changes to unstable [Fig. 5(e)] as the pH values increases. For nonmetal oxides, as shown in Fig. 5(d) and given in Table S1 [13,14,16–97], the photodecomposition-oxidative reactions with a much more negative ϕ^{ox} than $\phi^0(O_2/H_2O)$ lead to self-decomposition. Increasing the pH value will be unlikely to make them stable, although the pH dependence of their band-edge potentials is complicated.

In this work, our finding is that the highest possible VB-edge potential in stable photocatalysts is limited by photocorrosion at 2.48 V vs NHE at pH = 0 (called the PLL with $\phi^{PLL}=2.48$ V vs NHE). Because the potential of the CB edge must be more negative than the HER potential $\phi^0(H^+/H_2)$, which is 0 vs NHE at pH = 0, the limit of the photocorrosion-resistant photocatalysts with the highest VB potential at 2.48 V will exclude PEC photocatalysts from materials that have band gaps less than 2.48 eV. It is straightforward to learn that this predicted lower bound of the photocatalyst band gap can only be broken by a change of unstable photocatalysts having band gaps less than 2.48 eV to stable. For semiconducting photocatalysts with VB edges below $\phi^{PLL}=2.48$ V vs NHE at pH = 0, varying the pH value will not change the limit of the 2.48 eV minimum band gap for photocatalysts whenever they occur a change from unstable to stable. Nonmetal-oxide photocatalysts, as discussed above, will not undergo a change from unstable to stable upon increasing the pH value and thus, their pH dependence will not break the lower bound of the photocatalyst band gap imposed by photocorrosion. For metal oxides, although the VB edges rise up to a rate of -0.059 V/pH when increasing the pH value, this photocorrosion-limited minimum band gap will not change if the stabilities of all metal oxides do not change, because $\phi^0(H^+/H_2)$, which sets the limit of the CB edges of photocatalysts, also rises up with the same rate as the VB edges, as shown in Fig. 5(a) for the simplest case in BiOI where all pH-dependent lines of related potentials are parallel to each other. For metal-oxide photocatalysts as shown in Fig. 5(c), but with VB edges above $\phi^{PLL}=2.48$ V vs NHE at pH = 0, a change from unstable to stable with increasing pH value will break this limit. However, we do not find a case in Table S1 [13,14,16–97] where this happens, because for the cases as shown in Fig. 5(c), all metal-oxide and nonmetal-oxide semiconducting photocatalysts have too negative decomposition-oxidative potentials relative to $\phi^0(O_2/H_2O)$ to cross over with $\phi^0(O_2/H_2O)$ when increasing the pH value. Therefore, the conclusion drawn at pH = 0 is also applicable to a nonzero pH value.

[1] M. Grätzel, Photoelectrochemical cells, Nature **414**, 338 (2001).

[2] M. G. Walter, E. L. Warren, J. R. McKone, S. W. Boettcher, Q. Mi, E. A. Santori, and N. S. Lewis, Solar water splitting cells, Chem. Rev. **110**, 6446 (2010).

[3] F. E. Osterloh and B. A. Parkinson, Recent developments in solar water-splitting photocatalysis, MRS Bull. **36**, 17 (2011).

[4] T. Hisatomi, J. Kubota, and K. Domen, Recent advances in semiconductors for photocatalytic and photoelectrochemical water splitting, Chem. Soc. Rev. **43**, 7520 (2014).

[5] J. W. Ager, M. R. Shaner, K. A. Walczak, I. D. Sharp, and S. Ardo, Experimental demonstrations of spontaneous, solar-driven photoelectrochemical water splitting, Energ. Environ. Sci. **8**, 2811 (2015).

[6] M. J. Kenney, M. Gong, Y. Li, J. Z. Wu, J. Feng, M. Lanza, and H. Dai, High-performance silicon photoanodes passivated with ultrathin nickel films for water oxidation, Science **342**, 836 (2013).

[7] J. Gu, Y. Yan, J. L. Young, K. X. Steirer, N. R. Neale, and J. A. Turner, Water reduction by a p-GaInP2 photoelectrode stabilized by an amorphous TiO_2 coating and a molecular cobalt catalyst, Nat. Mater. **15**, 456 (2015).

[8] I. E. Castelli, T. Olsen, S. Datta, D. D. Landis, S. Dahl, K. S. Thygesen, and K. W. Jacobsen, Computational screening of perovskite metal oxides for optimal solar light capture, Energ. Environ. Sci. **5**, 5814 (2012).

[9] Y. Wu, P. Lazic, G. Hautier, K. Persson, and G. Ceder, First principles high throughput screening of oxynitrides for water-splitting photocatalysts, Energ. Environ. Sci. **6**, 157 (2013).

[10] S. Chen and L. W. Wang, Thermodynamic oxidation and reduction potentials of photocatalytic semiconductors in aqueous solution, Chem. Mater. **24**, 3659 (2012).

[11] H. Gerischer, On the stability of semiconductor electrodes against photodecomposition, J. Electroanal. Chem. Interf. Electrochem. **82**, 133 (1977).

[12] A. Paracchino, V. Laporte, K. Sivula, M. Grätzel, and E. Thimsen, Highly active oxide photocathode for photoelectrochemical water reduction, Nat. Mater. **10**, 456 (2011).

[13] Y. Xu and M. A. A. Schoonen, The absolute energy positions of conduction and valence bands of selected semiconducting minerals, Am. Mineral. **85**, 543 (2000).

[14] A. Kudo and Y. Miseki, Heterogeneous photocatalyst materials for water splitting, Chem. Soc. Rev. **38**, 253 (2009).

[15] X. Chen, S. Shen, L. Guo, and S. S. Mao, Semiconductor-based photocatalytic hydrogen generation, Chem. Rev. **110**, 6503 (2010).

[16] See Supplemental Material at http://link.aps.org/supplemental/10.1103/PhysRevApplied.10.064059 for details of the predicted photodecomposition lowest reductive and highest oxidative potentials and reactions for all 202 known semiconducting photocatalysts.

[17] L. Ye, Y. Su, X. Jin, H. Xie, and C. Zhang, Recent advances in BiOX (X=Cl, Br and I) photocatalysts: synthesis, modification, facet effects and mechanisms, Environ. Sci-Nano **1**, 90 (2014).

[18] Giménez and J. Bisquert, *Photoelectrochemical Solar Fuel Production* (Springer, Switzerland, 2016).

[19] A. B. Ellis, S. W. Kaiser, J. M. Bolts, and M. S. Wrighton, Study of n-type semiconducting cadmium chalcogenide-based photoelectrochemical cells employing polychalcogenide electrolytes, J. Am. Chem. Soc. **99**, 2839 (1977).

[20] N. E. Christensen and O. B. Christensen, Electronic structure of ZnTe and CdTe under pressure, Phys. Rev. B **33**, 4739 (1986).

[21] J. W. Jang, S. H. Cho, G. Magesh, Y. J. Jang, J. Y. Kim, W. Y. Kim, J. K. Seo, S. J. Kim, K. H. Lee, and J. S. Lee, Aqueous-solution route to zinc telluride films for application to CO_2 reduction, Angew. Chem. Int. Ed. **53**, 5852 (2014).

[22] G. H. Schoenmakers, Electroless etching of ZnSe in aqueous ferricyanide solutions, J. Electrochem. Soc. **144**, 2329 (1997).

[23] M. Long, W. M. Cai, and H. Kisch, Visible light induced photoelectrochemical properties of n-$BiVO_4$ and n-$BiVO_4$/p-Co_3O_4, J. Phys. Chem. C **112**, 548 (2008).

[24] Y. Matsumoto, M. Omae, K. Sugiyama, and E. Sato, New photocathode materials for hydrogen evolution: calcium iron oxide ($CaFe_2O_4$) and strontium iron oxide ($Sr_7Fe_{10}O_{22}$), J. Phys. Chem. C **91**, 577 (1987).

[25] M. Sugiyama, K. Fujii, and S. Nakamura, *Solar to Chemical Energy Conversion* (Springer, Heidelberg, 2016), Vol. 32, Lecture Notes in Energy.

[26] B. Tell, J. L. Shay, and H. M. Kasper, Electrical properties, optical properties, and band structure of $CuGaS_2$and $CuInS_2$, Phys. Rev. B **4**, 2463 (1971).

[27] H. Kato, K. Ueda, M. Kobayashi, and M. Kakihana, Photocatalytic water oxidation under visible light by valence band controlled oxynitride solid solutions $LaTaON_2$–$SrTiO_3$, J. Mater. Chem. A **3**, 11824 (2015).

[28] B. B. Kale, J. O. Baeg, S. M. Lee, H. Chang, S. J. Moon, and C. W. Lee, $CdIn_2S_4$ nanotubes and "marigold" nanostructures: A visible-light photocatalyst, Adv. Funct. Mater. **16**, 1349 (2006).

[29] B. Kumar, M. Llorente, J. Froehlich, T. Dang, A. Sathrum, and C. P. Kubiak, Photochemical and photoelectrochemical reduction of CO_2, Annu. Rev. Phys. Chem. **63**, 541 (2012).

[30] S. Vepřek, The search for novel, superhard materials, J. Vac. Sci. Technol A **17**, 2401 (1999).

[31] J. Zhang, J. Sun, K. Maeda, K. Domen, P. Liu, M. Antonietti, X. Fu, and X. Wang, Sulfur-mediated synthesis of carbon nitride: Band-gap engineering and improved functions for photocatalysis, Energ. Environ. Sci. **4**, 675 (2011).

[32] Y. Nakabayashi, M. Nishikawa, and Y. Nosaka, Fabrication of $CuBi_2O_4$ photocathode through novel anodic electrodeposition for solar hydrogen production, Electrochim. Acta **125**, 191 (2014).

[33] J. S. Jang, S. H. Choi, N. Shin, C. Yu, and J. S. Lee, $AgGaS_2$-type photocatalysts for hydrogen production under visible light: Effects of post-synthetic H_2S treatment, J. Solid State Chem. **180**, 1110 (2007).

[34] H. G. Kim, P. H. Borse, J. S. Jang, E. D. Jeong, O. S. Jung, Y. J. Suh, and J. S. Lee, Fabrication of $CaFe_2O_4$/$MgFe_2O_4$ bulk heterojunction for enhanced visible light photocatalysis, Chem. Commun. (Camb) **39**, 5889 (2009).

[35] I. Tsuji, Y. Shimodaira, H. Kato, H. Kobayashi, and A. Kudo, Novel stannite-type complex sulfide photocatalysts AI_2-Zn-AIV-S_4(AI=Cu and Ag; AIV=Sn and Ge) for hydrogen evolution under visible-light irradiation, Chem. Mater. **22**, 1402 (2010).

[36] N. T. Hahn, S. Hoang, J. L. Self, and C. B. Mullins, Spray pyrolysis deposition and photoelectrochemical properties of n-type BiOI nanoplatelet thin films, ACS Nano **6**, 7712 (2012).

[37] Y. Wang, Y. Wang, and Y. Gao, Photocatalytic H_2 evolution from water in the presence of carbon dioxide over NiO/$Ca_2Fe_2O_5$, React. Kinet. Mech. Catal. **99**, 485 (2010).

[38] T. Minegishi, N. Nishimura, J. Kubota, and K. Domen, Photoelectrochemical properties of $LaTiO_2N$ electrodes prepared by particle transfer for sunlight-driven water splitting, Chem. Sci. **4**, 1120 (2013).

[39] G. Hitoki, T. Takata, J. N. Kondo, M. Hara, H. Kobayashi, and K. Domen, An oxynitride, TaON, as an efficient water oxidation photocatalyst under visible light irradiation ($\lambda \leq 500$ nm), Chem. Commun., **16**, 1698 (2002).

[40] S. Balaz, S. H. Porter, P. M. Woodward, and L. J. Brillson, Electronic structure of tantalum oxynitride perovskite photocatalysts, Chem. Mater. **25**, 3337 (2013).

[41] M. Higashi, Y. Yamanaka, O. Tomita, and R. Abe, Fabrication of cation-doped $BaTaO_2N$ photoanodes for efficient photoelectrochemical water splitting under visible light irradiation, APL Mater. **3**, 104418 (2015).

[42] G. Hitoki, A. Ishikawa, T. Takata, J. N. Kondo, M. Hara, and K. Domen, Ta_3N_5 as a novel visible light-driven photocatalyst ($\lambda < 600$ nm), Chem. Lett. **31**, 736 (2002).

[43] A. Ishikawa, T. Takata, T. Matsumura, J. N. Kondo, M. Hara, H. Kobayashi, and K. Domen, Oxysulfides $Ln_2Ti_2S_2O_5$ as stable photocatalysts for water oxidation and reduction under visible-light irradiation, J. Phys. Chem. B **108**, 2637 (2004).

[44] R. Dom, A. S. Chary, R. Subasri, N. Y. Hebalkar, and P. H. Borse, Solar hydrogen generation from spinel $ZnFe_2O_4$ photocatalyst: effect of synthesis methods, Int. J. Energ. Res. **39**, 1378 (2015).

[45] S. Wang, D. Li, C. Sun, S. Yang, Y. Guan, H. He, R. Dom, A. S. Chary, R. Subasri, N. Y. Hebalkar, and P. H. Borse, Synthesis and characterization of g-C_3N_4/Ag_3VO_4 composites with significantly enhanced visible-light photocatalytic activity for triphenylmethane dye degradation, Appl. Catal. B: Environ. **144**, 885 (2014).

[46] H. Jeong, T. Kim, D. Kim, and K. Kim, Hydrogen production by the photocatalytic overall water splitting on NiO/$Sr_3Ti_2O_7$ NiO/$Sr_3Ti_2O_7$: Effect of preparation method, Int. J. Hydrogen Energy **31**, 1142 (2006).

[47] J. Yin, Z. Zou, and J. Ye, Photophysical and photocatalytic properties of new photocatalysts $MCrO_4$ (M=Sr, Ba), Chem. Phys. Lett. **378**, 24 (2003).

[48] Y. G. Ko and W. Y. Lee, Effects of nickel-loading method on the water-splitting activity of a layered NiO_x/$Sr_4Ti_3O_{10}$ photocatalyst, Catal. Lett. **83**, 157 (2002).

[49] H. Zhang, P. Yilmaz, J. O. Ansari, F. F. Khan, R. Binions, S. Krause, and S. Dunn, Incorporation of Ag nanowires in $CuWO_4$ for improved visible light-induced photoanode performance, J. Mater. Chem. A **3**, 9638 (2015).

[50] S. J. A. Moniz, R. Quesada-Cabrera, C. S. Blackman, J. Tang, P. Southern, P. M. Weaver, and C. J. Carmalt, A simple, low-cost CVD route to thin films of $BiFeO_3$ for efficient water photo-oxidation, J. Mater. Chem. A **2**, 2922 (2014).

[51] J. Hu, W. Fan, W. Ye, C. Huang, and X. Qiu, Insights into the photosensitivity activity of BiOCl under visible light irradiation, Appl. Catal. B: Environ. **158-159**, 182 (2014).

[52] D. Wang, Z. Zou, and J. Ye, A new spinel-type photocatalyst $BaCr_2O_4$ for H_2 evolution under UV and visible light irradiation, Chem. Phys. Lett. **373**, 191 (2003).

[53] T. Mishima, M. Matsuda, and M. Miyake, Visible-light photocatalytic properties and electronic structure of Zr-based oxynitride, Zr_2ON_2, derived from nitridation of ZrO_2, Appl. Catal. A: Gen. **324**, 77 (2007).

[54] M. Uno, A. Kosuga, M. Okui, K. Horisaka, H. Muta, K. Kurosaki, and S. Yamanaka, Photoelectrochemical study of lanthanide zirconium oxides, $Ln_2Zr_2O_7$ (Ln=La, Ce, Nd and Sm), J. Alloys Compd. **420**, 291 (2006).

[55] D. Li, J. Zheng, and Z. Zou, Band structure and photocatalytic properties of perovskite-type compound Ca_2NiWO_6 for water splitting, J. Phys. Chem. Solids **67**, 801 (2006).

[56] D. Wang, J. Tang, Z. Zou, and J. Ye, Photophysical and photocatalytic properties of a new series of visible-light-driven photocatalysts $M_3V_2O_8$(M=Mg, Ni, Zn), Chem. Mater. **17**, 5177 (2005).

[57] L. Ni, M. Tanabe, and H. Irie, A visible-light-induced overall water-splitting photocatalyst: conduction-band-controlled silver tantalate, Chem. Commun. (Camb) **49**, 10094 (2013).

[58] K. T. Jacob and G. Rajitha, Discussion of enthalpy, entropy and free energy of formation of GaN, J.Cryst. Growth **311**, 3806 (2009).

[59] J. F. Zhang and T. Zhang, Preparation and characterization of highly efficient and stable visible-light-responsive photocatalyst AgBr/Ag_3PO_4, J. Nanomater. **2013**, 1 (2013).

[60] J. Ye, Z. Zou, M. Oshikiri, A. Matsushita, M. Shimoda, M. Imai, and T. Shishido, A novel hydrogen-evolving photocatalyst $InVO_4$ active under visible light irradiation, Chem. Phys. Lett. **356**, 221 (2002).

[61] Q. P. Ding, Y. P. Yuan, X. Xiong, R. P. Li, H. B. Huang, Z. S. Li, T. Yu, Z. G. Zou, and S. G. Yang, Enhanced photocatalytic water splitting properties of $KNbO_3$ nanowires synthesized through hydrothermal method, J. Phys. Chem. C **112**, 18846 (2008).

[62] J. Ye, Z. G. Zou, and A. Matsushita, A novel series of water splitting photocatalysts NiM_2O_6 (M=Nb,Ta) active under visible light, Int. J. Hydrogen Energy **28**, 651 (2003).

[63] Z. Zou, J. Ye, and H. Arakawa, Photophysical and photocatalytic properties of $InMO_4$ ($M=Nb^{5+}$, Ta^{5+}) under visible light irradiation, Mater. Res. Bull. **36**, 1185 (2001).

[64] K. Iwashina, A. Iwase, and A. Kudo, Sensitization of wide band gap photocatalysts to visible light by molten CuCl treatment, Chem. Sci. **6**, 687 (2015).

[65] D. W. Hwang, J. S. Lee, W. Li, and S. H. Oh, Electronic band structure and photocatalytic activity of $Ln_2Ti_2O_7$(Ln=La, Pr, Nd), J. Phys. Chem. B **107**, 4963 (2003).

[66] Z. Zhang, J. B. Goodall, S. Brown, L. Karlsson, R. J. Clark, J. L. Hutchison, I. U. Rehman, and J. A. Darr, Continuous hydrothermal synthesis of extensive 2D sodium titanate ($Na_2Ti_3O_7$) nano-sheets, Dalton Trans. **39**, 711 (2010).

[67] S. A. Khana, I. A. Khana, M. S. Khanb, M. Zaherab, and M. Arshadc, $Na_2Ti_6O_{13}$ belts: A comparative study on structural, optical and morphological properties prepared by sol-gel and solid state reaction routes, Arch. Appl. Sci. Res. **7**, 42 (2015).

[68] H. G. Kim, O. S. Becker, J. S. Jang, S. M. Ji, P. H. Borse, and J. S. Lee, A generic method of visible light sensitization for perovskite-related layered oxides: Substitution effect of lead, J. Solid State Chem. **179**, 1214 (2006).

[69] Y. Wang, Z. Zhang, Y. Zhu, Z. Li, R. Vajtai, L. Ci, and P. M. Ajayan, Nanostructured VO_2 photocatalysts for hydrogen production, ACS Nano **2**, 1492 (2008).

[70] J. Sheng, X. Li, and Y. Xu, Generation of H_2O_2 and OH radicals on Bi_2WO_6 for phenol degradation under visible light, ACS Catal. **4**, 732 (2014).

[71] G. H. Du, Q. Chen, P. D. Han, Y. Yu, and L. M. Peng, Potassium titanate nanowires: Structure, growth, and optical properties, Phys. Rev. B **67**, 035323 (2003).

[72] X. Tu, S. Luo, G. Chen, and J. Li, One-pot synthesis, characterization, and enhanced photocatalytic activity of a BiOBr–graphene composite, Chemistry **18**, 14359 (2012).

[73] G. Li, T. Kako, D. Wang, Z. Zou, and J. Ye, Synthesis and enhanced photocatalytic activity of $NaNbO_3$ prepared by hydrothermal and polymerized complex methods, J. Phys. Chem. Solids **69**, 2487 (2008).

[74] Z. Wang, Z. Quan, and J. Lin, Remarkable changes in the optical properties of CeO_2 nanocrystals induced by lanthanide ions doping, Inorg. Chem. **46**, 5237 (2007).

[75] C. Huang, C. H. Cheng, K. T. Lee, and B. H. Liou, High-performance metal-insulator-metal capacitor using quality properties of high-K TiPrO dielectric, J. Electrochem. Soc. **156**, G23 (2009).

[76] I. A. Mkhalid, Visible light photocatalytic synthesis of aniline with an Au/$LaTiO_3$ nanocomposites, J.Alloys Compd. **631**, 298 (2015).

[77] P. Kanhere, J. Zheng, and Z. Chen, Visible light driven photocatalytic hydrogen evolution and photophysical properties of Bi^{3+} doped $NaTaO_3$, Int. J. Hydrogen Energy **37**, 4889 (2012).

[78] Z. Zou, J. Ye, K. Sayama, and H. Arakawa, Photocatalytic and photophysical properties of a novel series of solid photocatalysts, $BiTa_{1-x}Nb_xO_4$ ($0 \leq x \leq 1$), Chem. Phys. Lett. **343**, 303 (2001).

[79] Y. Miseki, H. Kato, and A. Kudo, Water splitting into H_2 and O_2 over niobate and titanate photocatalysts with (111) plane-type layered perovskite structure, Energ. Environ. Sci. **2**, 306 (2009).

[80] I. S. Cho, C. H. Kwak, D. W. Kim, S. Lee, and K. S. Hong, Photophysical, photoelectrochemical, and photocatalytic properties of novel $SnWO_4$ oxide semiconductors with narrow band gaps, J. Phys. Chem. C **113**, 10647 (2009).

[81] W. F. Zhang, J. Tang, and J. Ye, Photoluminescence and photocatalytic properties of $SrSnO_3$ perovskite, Chem. Phys. Lett. **418**, 174 (2006).

[82] K. C. Leonard, K. M. Nam, H. C. Lee, S. H. Kang, H. S. Park, and A. J. Bard, $ZnWO_4/WO_3$ composite for improving photoelectrochemical water oxidation, J. Phys. Chem. C **117**, 15901 (2013).

[83] B. Prijamboedi, S. Umar, and F. Failamani, Electronic structure and optical properties of Sr_2SnO_4 studied with FP-LAPW method in density functional theory, AIP Conf. Proc. **1656**, 030001 (2015).

[84] Y. Hosogi, Y. Shimodaira, H. Kato, H. Kobayashi, and A. Kudo, Role of Sn^{2+} in the band structure of SnM_2O_6 and $Sn_2M_2O_7$(M=Nb and Ta) and their photocatalytic properties, Chem. Mater. **20**, 1299 (2008).

[85] Y. Yamashita, M. Tada, M. Kakihana, M. Osada, and K. Yoshida, Synthesis of RuO_2-loaded $BaTi_nO_{2n+1}$ (n=1, 2 and 5) using a polymerizable complex method and its photocatalytic activity for the decomposition of water, J. Mater.Chem. **12**, 1782 (2002).

[86] K. Kawashima, M. Hojamberdiev, H. Wagata, K. Yubuta, S. Oishi, and K. Teshima, Chloride flux growth of La_2TiO_5 crystals and nontopotactic solid-state transformation to $LaTiO_2N$ crystals by nitridation using NH_3, Cryst. Growth Des. **15**, 333 (2015).

[87] J. Tang, Z. Zou, and J. Ye, Photophysical and photocatalytic properties of $AgInW_2O_8$, J. Phys. Chem. B **107**, 14265 (2003).

[88] K. Yoshioka, V. Petrykin, M. Kakihana, H. Kato, and A. Kudo, The relationship between photocatalytic activity and crystal structure in strontium tantalates, J. Catal. **232**, 102 (2005).

[89] D. Chen and J. Ye, Selective-synthesis of high-performance single-crystalline $Sr_2Nb_2O_7$ nanoribbon and $SrNb_2O_6$ nanorod photocatalysts, Chem. Mater. **21**, 2327 (2009).

[90] Y. Li, G. Chen, H. Zhang, Z. Li, and J. Sun, Electronic structure and photocatalytic properties of $ABi_2Ta_2O_9$ (A=Ca, Sr, Ba), J. Solid State Chem. **181**, 2653 (2008).

[91] M. Machida, S. Murakami, T. Kijima, S. Matsushima, and M. Arai, Photocatalytic property and electronic structure of lanthanide tantalates, $LnTaO_4$(Ln=La, Ce, Pr, Nd, and Sm), J. Phys. Chem. B **105**, 3289 (2001).

[92] C. S. Enache, D. Lloyd, M. R. Damen, J. Schoonman, and R. van de Krol, Photo-electrochemical properties of thin-film $InVO_4$ photoanodes: The role of deep donor states, J. Phys. Chem. C **113**, 19351 (2009).

[93] J. Sato, N. Saito, Y. Yamada, K. Maeda, T. Takata, J. N. Kondo, M. Hara, H. Kobayashi, K. Domen, and Y. Inoue, RuO_2-loaded beta-Ge_3N_4 as a non-oxide photocatalyst for overall water splitting, J. Am. Chem. Soc. **127**, 4150 (2005).

[94] Y. Yuan, X. Zhang, L. Liu, X. Jiang, J. Lv, Z. Li, and Z. Zou, Synthesis and photocatalytic characterization of a new photocatalyst $BaZrO_3$, Int. J. Hydrogen Energy **33**, 5941 (2008).

[95] X. Chen, T. Yu, X. Fan, H. Zhang, Z. Li, J. Ye, and Z. Zou, Enhanced activity of mesoporous Nb_2O_5 for photocatalytic hydrogen production, Appl. Surf. Sci. **253**, 8500 (2007).

[96] L. Sun, Y. Qi, C. J. Jia, Z. Jin, and W. Fan, Enhanced visible-light photocatalytic activity of g-C_3N_4/Zn_2GeO_4 heterojunctions with effective interfaces based on band match, Nanoscale **6**, 2649 (2014).

[97] H. Kato and A. Kudo, New tantalate photocatalysts for water decomposition into H_2 and O_2, Chem. Phys. Lett. **295**, 487 (1998).

[98] A. Fujishima and K. Honda, Electrochemical photolysis of water at a semiconductor electrode, Nature **238**, 37 (1972).

[99] H. Kazuhito, I. Hiroshi, and F. Akira, TiO_2 photocatalysis: A historical overview and future prospects, Jpn. J. Appl. Phys. **44**, 8269 (2005).

[100] Y. Park, K. J. McDonald, and K. S. Choi, Progress in bismuth vanadate photoanodes for use in solar water oxidation, Chem. Soc. Rev. **42**, 2321 (2013).

[101] A. Kudo, K. Omori, and H. Kato, A novel aqueous process for preparation of crystal form-controlled and highly crystalline $BiVO_4$ powder from layered vanadates at room temperature and its photocatalytic and photophysical properties, J. Am. Chem. Soc. **121**, 11459 (1999).

[102] J. A. Seabold and K. S. Choi, Efficient and stable photooxidation of water by a bismuth vanadate photoanode coupled with an iron oxyhydroxide oxygen evolution catalyst, J. Am. Chem. Soc. **134**, 2186 (2012).

[103] Z. G. Yi, J. H. Ye, N. Kikugawa, T. Kako, S. Ouyang, H. S. Williams, H. Yang, J. Y. Cao, W. J. Luo, Z. S. Li, Y. Liu, and R. L. Withers, An orthophosphate semiconductor with photooxidation properties under visible-light irradiation, Nat. Mater. **9**, 559 (2010).

[104] X. Chen, Y. Dai, and X. Wang, Methods and mechanism for improvement of photocatalytic activity and stability of Ag_3PO_4: A review, J. Alloys Compd. **649**, 910 (2015).

[105] Y. Lee, T. Watanabe, T. Takata, M. Hara, M. Yoshimura, and K. Domen, Effect of high-pressure ammonia treatment on the activity of Ge_3N_4 photocatalyst for overall water splitting, J. Phys. Chem. B **110**, 17563 (2006).

[106] D. S. Bhachu, S. J. A. Moniz, S. Sathasivam, D. O. Scanlon, A. Walsh, S. M. Bawaked, M. Mokhtar, A. Y. Obaid, I. P. Parkin, J. W. Tang, and C. J. Carmalt, Bismuth oxyhalides: Synthesis, structure and photoelectrochemical activity, Chem. Sci. **7**, 4832 (2016).

[107] K. Maeda and K. Domen, Oxynitride materials for solar water splitting, MRS Bull. **36**, 25 (2011).
[108] T. Takata, C. Pan, and K. Domen, Recent progress in oxynitride photocatalysts for visible-light-driven water splitting, Sci. Technol. Adv. Mater. **16**, 033506 (2015).
[109] X. Chen, L. Liu, P. Y. Yu, and S. S. Mao, Increasing solar absorption for photocatalysis with black hydrogenated titanium dioxide nanocrystals, Science **331**, 746 (2011).
[110] H. X. Deng, S. S. Li, J. Li, and S. H. Wei, Effect of hydrogen passivation on the electronic structure of ionic semiconductor nanostructures, Phys. Rev. B **85**, 195328 (2012).
[111] Y. H. Hu, A highly efficient photocatalyst–hydrogenated black TiO_2 for the photocatalytic splitting of water, Angew. Chem. Int. Ed. **51**, 12410 (2012).
[112] T. A. Pham, Y. Ping, and G. Galli, Modelling heterogeneous interfaces for solar water splitting, Nat. Mater. **16**, 401 (2017).
[113] J. R. Bolton, S. J. Strickler, and J. S. Connolly, Limiting and realizable efficiencies of solar photolysis of water, Nature **316**, 495 (1985).
[114] K. T. Fountaine, H. J. Lewerenz, and H. A. Atwater, Efficiency limits for photoelectrochemical water-splitting, Nat. Commun. **7**, 13706 (2016).
[115] W. Shockley and H. J. Queisser, Detailed balance limit of efficiency of p-n junction solar cells, J. Appl. Phys. **32**, 510 (1961).
[116] M. A. Butler and D. S. Ginley, Prediction of flatband potentials at semiconductor-electrolyte interfaces from atomic electronegativities, J. Electrochem. Soc. **125**, 228 (1978).
[117] J. Portier, G. Campet, C. W. Kwon, J. Etourneau, and M. A. Subramanian, Relationships between optical band gap and thermodynamic properties of binary oxides, Int. J. Inorg. Mater. **3**, 1091 (2001).
[118] A. G. Scheuermann, J. P. Lawrence, K. W. Kemp, T. Ito, A. Walsh, C. E. D. Chidsey, P. K. Hurley, and P. C. McIntyre, Design principles for maximizing photovoltage in metal-oxide-protected water-splitting photoanodes, Nat. Mater. **15**, 99 (2015).
[119] K. Sun, F. H. Saadi, M. F. Lichterman, W. G. Hale, H. P. Wang, X. H. Zhou, N. T. Plymale, S. T. Omelchenko, J. H. He, K. M. Papadantonakis, B. S. Brunschwig, and N. S. Lewis, Stable solar-driven oxidation of water by semiconducting photoanodes protected by transparent catalytic nickel oxide films, Proc. Natl. Acad. Sci. **112**, 3612 (2015).
[120] R. Liu, Z. Zheng, J. Spurgeon, and X. Yang, Enhanced photoelectrochemical water-splitting performance of semiconductors by surface passivation layers, Energ. Environ. Sci. **7**, 2504 (2014).
[121] Y. Yang, J. Gu, J. L. Young, E. M. Miller, J. A. Turner, N. R. Neale, and M. C. Beard, Semiconductor interfacial carrier dynamics via photoinduced electric fields, Science **350**, 1061 (2015).
[122] H. Gerischer, Electrolytic decomposition and photodecomposition of compound semiconductors in contact with electrolytes, J. Vac. Sci. Technol. **15**, 1422 (1978).
[123] A. J. Bard and M. S. Wrighton, Thermodynamic potential for the anodic dissolution of n-type semiconductors, J. Electrochem Soc. **124**, 1706 (1977).
[124] E. M. Miller, D. M. Kroupa, J. B. Zhang, P. Schulz, A. R. Marshall, A. Kahn, S. Lany, J. M. Luther, M. C. Beard, C. L. Perkins, and J. V. D. Lagemaat, Revisiting the valence and conduction band size dependence of PbS quantum dot thin films, ACS Nano **10**, 3302 (2016).
[125] W. J. Chun, A. Ishikawa, H. Fujisawa, T. Takata, J. N. Kondo, M. Hara, M. Kawai, Y. Matsumoto, and K. Domen, Conduction and valence band positions of Ta_2O_5, TaON, and Ta_3N_5 by UPS and electrochemical methods, J. Phys. Chem. B **107**, 1798 (2003).
[126] J. Cheng and M. Sprik, Alignment of electronic energy levels at electrochemical interfaces, Phys. Chem. Chem. Phys. **14**, 11245 (2012).
[127] *CRC Handbook of Chemistry and Physics: A Ready-Reference Book of Chemical and Physical Data*. 83. ed., 2002 - 2003 ed. 2002 (CRC Press, Boca Raton, FL).
[128] *Lange's Handbook of Chemistry* (McGraw-Hill, New York, NY, 1999), 15th ed. McGraw-Hill handbooks.
[129] V. Stevanović, S. Lany, X. Zhang, and A. Zunger, Correcting density functional theory for accurate predictions of compound enthalpies of formation: Fitted elemental-phase reference energies, Phys. Rev. B **85**, 115104 (2012).
[130] J. Portier, H. Hilal, I. Saadeddin, S. Hwang, M. Subramanian, and G. Campet, Thermodynamic correlations and band gap calculations in metal oxides, Prog. Solid State Chem. **32**, 207 (2004).
[131] E. D. Verink Jr., *Uhlig's corrosion handbook*, in *Electrochemical Society series* (Wiley, New York, 2000), p. 111.